Takabayashi et al. EURASIP Journal on Wireless Communications and Networking (2016) 2016:70
DOI 10.1186/s13638-016-0561-0

EURASIP Journal on Wireless Communications and Networking
a SpringerOpen Journal

RESEARCH Open Access

Performance analysis of multiplexing and error control scheme for body area networks

Kento Takabayashi[1*], Hirokazu Tanaka[2], Chika Sugimoto[1] and Ryuji Kohno[1]

Abstract

In this paper, we theoretically analyze the performance of a multiplexing and error control scheme for body area networks. In our previous work, we proposed a quality of service (QoS) control optimization method that achieves optimal QoS control by introducing a multiplexing scheme over the media access control (MAC) layer. This multiplexing scheme combines Weldon-based hybrid automatic repeat request (ARQ) with a decomposable error-correcting code. In this paper, we present a theoretical analysis of our proposed scheme as an extension of our previous work. In this proposed system, the decomposable code which has simpler structure is utilized. We then show that our proposed multiplexing layer can achieve optimal performance at $E_s/N_0 = 3$, 5, and 6 dB in the additive white Gaussian noise (AWGN) channel and at $E_s/N_0 = 8$, 11, and 14 dB in the Rayleigh fading channel by arbitrarily selecting parameters for the error-correcting code and hybrid ARQ. Then, we show that the proposed system obtains over 1.2 dB gain in the AWGN channel and over 4.2 dB gain in the Rayleigh fading channel than IEEE802.15.6 in the optional pattern.

Keywords: Wearable sensor, Body area network, QoS control, Multiplexing

1 Introduction

Health monitoring systems that employ wearable vital sensors and wireless communication have recently received significant attention [1–16]. It is expected that wearable sensors will pave the way for a new era of tele-healthcare that may include continuous monitoring of physical conditions and the detection of serious consequences. In the field of health-monitoring systems, the body area network (BAN) is a key technology [1–4, 10–16]. Its standardization activities have been carried out extensively [17–19]. To realize smaller sensor devices and longer battery life, the following technical requirements should be considered.

- Ultra-low power consumption
  Although this has been considered in the above standards, substantially lower power-consuming media access control (MAC) and physical layer (PHY) technologies are required.
- Coexistence with other networks
  The 2.4-GHz industrial, scientific, and medical (ISM) band is globally assigned for common use in local area network (LAN) and personal area network (PAN) devices. This frequency band is potentially a good candidate for BANs; however, when using this band, interference from other systems must be taken into consideration.
- Optimal quality of service (QoS) control
  A wearable vital sensor can connect various types of sensors, with the data rate of such sensors varying widely. Further, their respective allowable delay times depend on their application. Therefore, optimal QoS control for input data is an important factor in transmitting sensor data.

From the above requirements, we have proposed an optimal QoS control scheme that employs a multiplexing layer and a decomposable error control coding scheme [20–22]. In [20], we proposed a QoS control

* Correspondence: takabayashi-kento-xp@ynu.jp
[1]Graduate School of Engineering, Yokohama National University, 79-5 Tokiwadai, Hodogaya-Ku, 240-8501 Yokohama, Japan
Full list of author information is available at the end of the article

scheme using Weldon-based hybrid automatic repeat request (ARQ) [23] with Reed-Muller codes. However, the error-correcting capability could not be increased effectively because of characteristics of Reed-Muller codes which we selected in [20]. So, we conducted simulations to evaluate the performance of the proposed system utilizing Weldon's ARQ with decomposable codes based on punctured convolutional codes in the additive white Gaussian noise (AWGN) channel [21] and a wearable BAN channel model [22] by comparing it with IEEE 802.15.6. Assuming that the wearable sensor device has multiple sensors, each sensor's input data are transmitted through a common MAC and PHY layer [21, 22].

Because we evaluated the effectiveness of our proposed scheme only via simulation in our previous work, in this paper, we present a theoretical analysis of our proposed scheme in [21] and [22] under the AWGN channel and the Rayleigh fading channel as an extension of our previous work. We have not evaluated and analyzed the case of the Rayleigh fading channel in our previous work. Then, in this proposed system, the structure of our decomposable code is modified to be much simpler than that in our previous work [21, 22] in order to analyze it more easily. In general, an evaluation of ARQ requires a large number of simulation trials to fully evaluate the given system; however, we can specifically evaluate the throughput in a stable state by sound theoretical analysis. More specifically, we can easily obtain detailed characteristics of our proposed scheme by this formulization. We derived a lower bound on throughput performance and an upper bound on residual bit error rate in the AWGN channel and the Rayleigh fading channel. In addition, we investigated QoS parameters to further optimize our system. For example, we identified the optimum parameters according to various policies, as shown in Tables 3 and 4. Figure 8 shows the results of our throughput optimization by using the parameters of Table 4.

The remainder of this paper is organized as follows. In Section 2, we briefly review the system model of our proposed scheme. Section 3 explains the theoretical analysis of our proposed scheme under the AWGN channel and the Rayleigh fading channel. Performance evaluations by theoretical analysis and simulations are presented in Section 4. Finally, we conclude our paper and provide directions for future work in Section 5.

2 System model

2.1 System concept

Figure 1 shows the overall concept of our proposed system. In general, different types of data are input and multiplexed at a single sensor device [19]. Here, we assume that the different types of data input and multiplexed have potentially different QoS requirements. Given the varying QoS requirements, the different types of data have different priorities. These data are multiplexed and transmitted from a sensor (i.e., a wireless body area network (WBAN) node) to a WBAN coordinator.

Figure 2 shows the system model. The transmitter consists of a multiplexing module, a MAC module, and a PHY module. The multiplexing module controls the different types of QoS requirements according to the following priorities. First, several data are added to user priorities. Then, the header, which includes user priority information (e.g., latency, rate of error control coding,

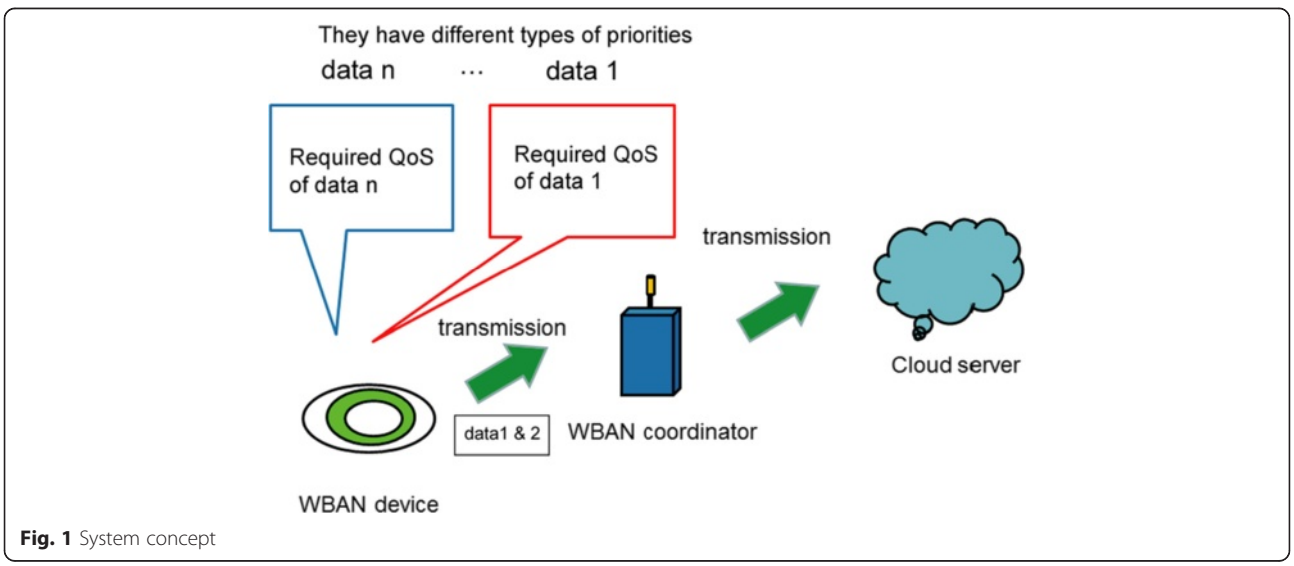

Fig. 1 System concept

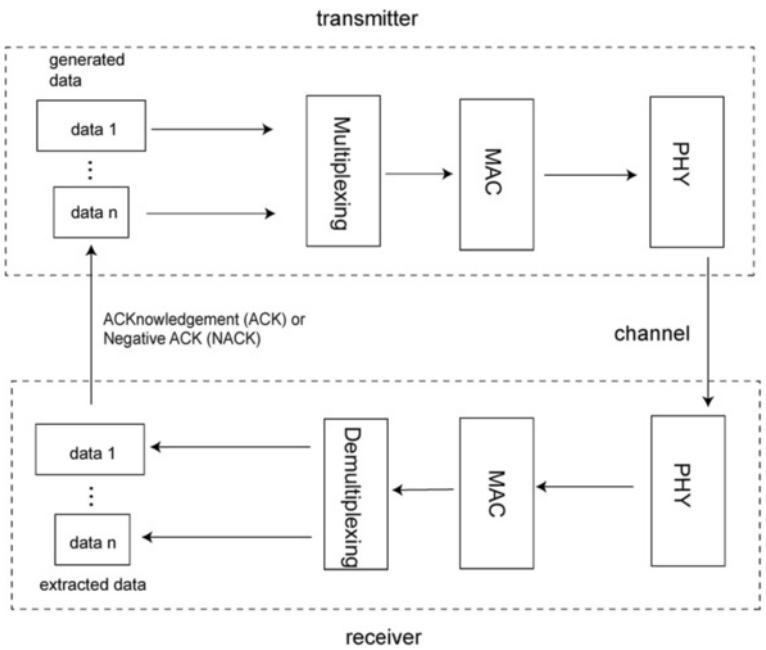

Fig. 2 System model of the proposed scheme

information m	m_1	m_2	m_3	m_4	m_5	m_6	m_7	m_8
output u_1	u_{11}	u_{12}	u_{13}	u_{14}	u_{15}	u_{16}	u_{17}	u_{18}
output u_2	u_{21}	u_{22}	u_{23}	u_{24}	u_{25}	u_{26}	u_{27}	u_{28}

punctured matrix

$$\begin{bmatrix} 1 & 1 & 0 & 1 & 0 & 1 & 0 & 1 \\ 1 & 0 & 1 & 0 & 1 & 0 & 1 & 0 \end{bmatrix}$$

information m	m_1	m_2	m_3	m_4	m_5	m_6	m_7	m_8
output u_1	u_{11}	u_{12}	×	u_{14}	×	u_{16}	×	u_{18}
output u_2	u_{21}	×	u_{23}	×	u_{25}	×	u_{27}	×

codeword 1 $\begin{bmatrix} u_{11} & u_{12} & u_{14} & u_{16} & u_{18} \\ u_{21} & u_{23} & u_{25} & u_{27} & \times \end{bmatrix}$

and

information m	m_1	m_2	m_3	m_4	m_5	m_6	m_7	m_8
output u_1	u_{11}	×	u_{13}	×	u_{15}	×	u_{17}	×
output u_2	u_{21}	u_{22}	×	u_{24}	×	u_{24}	×	u_{28}

codeword 1' $\begin{bmatrix} u_{11} & u_{13} & u_{15} & u_{17} & \times \\ u_{21} & u_{22} & u_{24} & u_{26} & u_{28} \end{bmatrix}$

Fig. 3 Punctured convolutional code

the number of repetitions in ARQ, etc.), is added to the user priorities in the multiplexing layer. Next, the multiplexer controller in the multiplexing layer provides instructions to each data depending on predefined parameters. According to the QoS control signal, the multiplexing layer performs error and delay control. Finally, data with different user priorities are multiplexed and sent to the MAC layer.

In the MAC module, the error control process is performed according to the instructions from the multiplexing module. In the PHY module, this multiplexed data is modulated. In this paper, coherent phase shift keying (PSK) is used for basic analysis. Then, direct sequence spread spectrum (DSSS) is applied to increase robustness against multipath fading and multiuser interference. At the receiver, the transmission operation is processed in the reverse order. Finally, after the process at the demultiplexing module is complete, error detection is performed on the data.

2.2 Decomposable code

In our proposed scheme, Weldon's ARQ [23] is employed rather than selective repeat ARQ, and decomposable code is employed as error-correction code for hybrid ARQ. The proposed scheme can provide an error control method that satisfies various QoS requirements by coordinating the number of data copies and changing how the decomposable code is combined.

As an example of decomposable code, a punctured convolutional code with constraint length K set to 3 and coding rates 8/9, 4/5, 2/3, and 1/2 is used. In [21] and [22], we selected coding rates 7/8, 5/6, 3/4, and 1/2. However, those punctured matrices in [21] and [22] are very complicated, and then it is very difficult to analyze its performance in theory. On the other hand, punctured matrices which we select in this paper are quite simple and can be analyzed more easily.

The punctured convolutional code is generated based on the convolutional code with a generator polynomial of [5, 7] and coding rate $R = 1/2$. The punctured matrix of $R = 8/9$ is shown in Fig. 3. The two patterns of the $R = 8/9$ punctured codes (codeword 1 and codeword 1′) can be generated using this punctured matrix. More specifically, at the first transmission, codeword 1 is sent; then, to increment the code rate of the punctured code, a part of codeword 1′ is sent as the second transmission. Figure 4

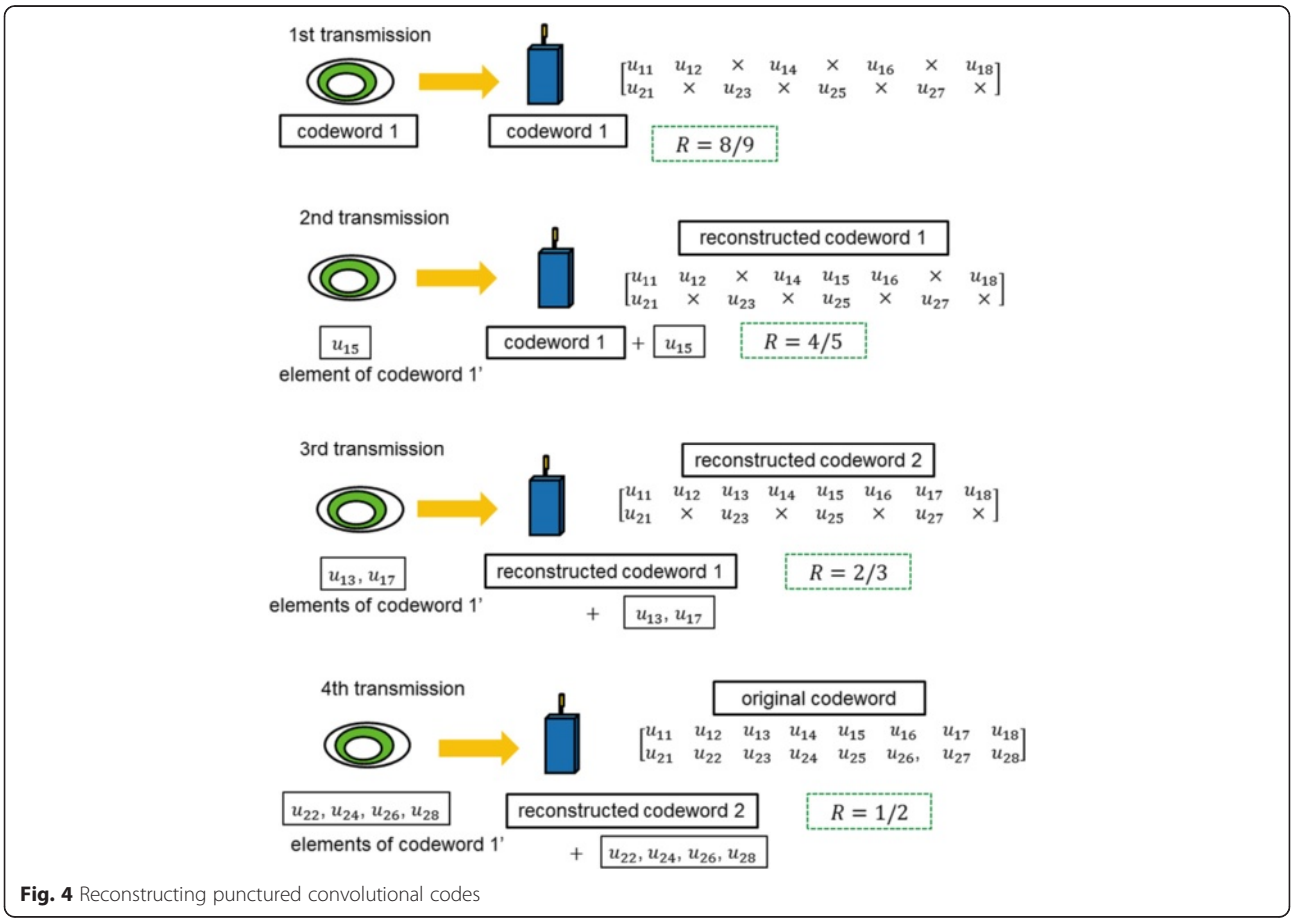

Fig. 4 Reconstructing punctured convolutional codes

illustrates how to increment redundancies and send the sub-codewords except u_{11} and u_{21} from the first transmission to the fourth transmission. As shown in the figure, these punctured matrices consist of a subset that is a part of the next punctured matrix. In general, at the ith retransmission, reconstructed codewords are decoded as error-correction codes with a coding rate set as follows:

$$R_{\mathrm{i}} = \begin{cases} 8/9\ (i=0) \\ 4/5\ (i=1) \\ 2/3\ (i=2) \\ 1/2\ (i \geq 3) \end{cases}. \tag{1}$$

The error-correction capability increases as the coding rate decreases in the order 8/9, 4/5, 2/3, and 1/2.

2.3 Procedure of the proposed scheme

Figure 5 shows a flowchart of the protocol for our proposed scheme. In the proposed method, retransmission is performed as follows. First, information m is encoded via the punctured convolutional code whose $R = 8/9$; then, codeword 1 in Fig. 4 is transmitted. If errors are detected, the receiver stores the transmitted codeword 1 and the transmitter re-sends the sub-codeword of codeword 1′ n_i times in the case $1 \leq i \leq 3$. At the receiver, a received sub-codeword and stored codeword are combined (Fig. 4), and the reconstructed codeword is decoded. After the third retransmission, codeword 1 is sent n_4 times and combined with a buffered codeword. If errors are detected, one of n_4 codeword 1 is buffered in the receiver, and codeword 1′ is transmitted n_5 times and combined with a stored codeword. After that, codeword 1 and codeword 1′ are sent alternately n_i times and stored. When codeword 1 or codeword 1′ is buffered, the first one among n_i copies is stored. The transmitter repeats these operations until the data is received correctly or the number of retransmissions reaches the predefined maximum number of retransmissions q.

3 Theoretical analysis

We define normalized throughput $\eta = k_0/T$ as the number of total communicated bits and uncoded bits k_0. The number of total communicated bits T is determined as follows:

$$T \cong \sum_{i=0}^{q} \prod_{j=0}^{i} P_{j-1}^{n_{j-1}} \left(1 - P_i^{n_i}\right) \left(\sum_{k=0}^{i} n_k m_k \right) + \sum_{j=0}^{q} n_j m_j \prod_{j=0}^{q} P_i^{n_i} \quad (* P_{-1} \equiv 1,\ n_{-1} \equiv 0). \tag{2}$$

Here, P_i is the packet error rate (PER), m_i is the number of transmitted bits, and n_i is the number of copy

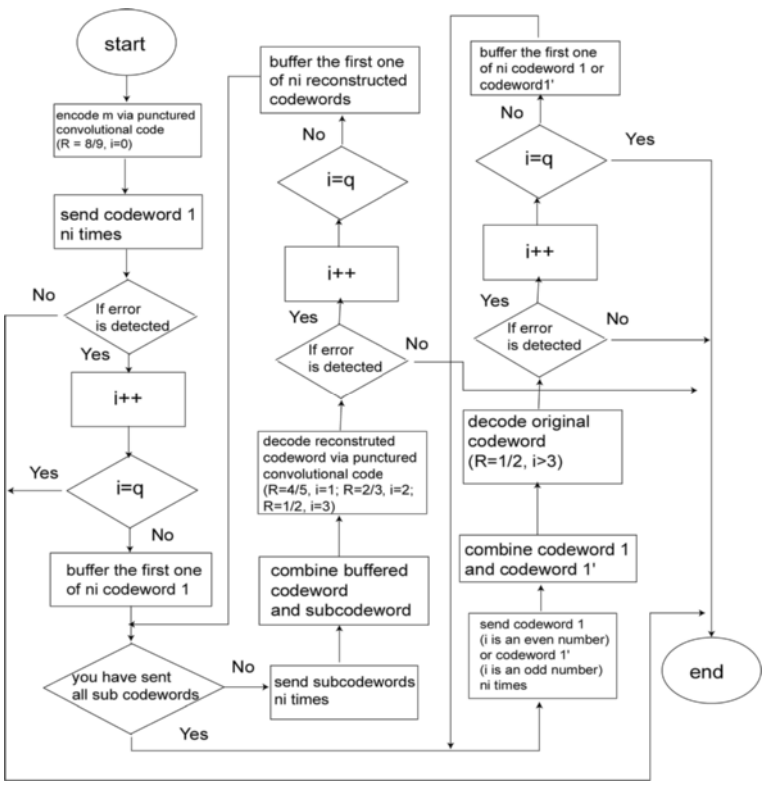

Fig. 5 Flowchart of the proposed ARQ protocol

blocks of Weldon's ARQ at the ith transmission. Then, P_i changes in stages because the received data is decoded by decomposable codes with coding rates varying in order of Eq. 1. Note that throughput T is described as the above approximate equation due to the maximum retransmission limit.

Next, we consider the upper bounds on error probability of the punctured convolutional codes used by the proposed scheme to obtain P_i. These bounds are obtained from the transfer function *T(D,N)* of the code, which describes the weight distribution or weight spectrum of the incorrect codewords and the number of bit errors on these paths [24]. The transfer function *T(D,N)* is expressed as follows:

$$T(D,N)|_{N=1} = \sum_{d=d_{free}}^{\infty} a_d D^d \tag{3}$$

$$\frac{dT(D,N)}{dN}\Big|_{N=1} = \sum_{d=d_{free}}^{\infty} c_d D^d. \tag{4}$$

Here, d_{free} is the free distance of the code, and a_d is the number of incorrect paths or adversaries of the Hamming weight d, $d \le d_{free}$. In addition, c_d is the total number of information bit errors produced by the incorrect paths of the Hamming weight.

Using *T(D,N)*, the upper bounds on the event error probability P_E and the bit error probability P_B of a code with rate $R_i = k/v$ are given as follows:

$$P_E \le \sum_{d=d_{free}}^{\infty} a_d P_d \tag{5}$$

$$P_B \le \frac{1}{k} \sum_{d=d_{free}}^{\infty} c_d P_d. \tag{6}$$

Here,

$$P_d = Q\left(\sqrt{2dR\frac{E_b}{N_0}}\right) \tag{7}$$

$$Q(x) = \int_x^{\infty} \frac{1}{2\pi} exp\left(-\frac{1}{2}z^2\right) dz\,. \tag{8}$$

Here, E_b/N_0 is the energy per bit-to-noise density ratio and P_d is the pairwise error probability in the case of PSK modulation and unquantized AWGN channels [25]. Then, in case of the Rayleigh fading channel, P_d is expressed as follows [26]:

$$P_d = (P_e)^d \sum_{t=0}^{d-1} \binom{d-1-t}{t} (1-P_e)^t \tag{9}$$

$$P_e = 1-\sqrt{\frac{\gamma_b R}{1+\gamma_b R}}, \tag{10}$$

where γ_b is the average of E_b/N_0.

Further, P_i is determined using P_B from the following equation:

$$P_i = 1-(1-P_B)^{L_{info}}. \tag{11}$$

Here, L_{info} is the number of information bits. In addition, the upper bound of the residual bit error rate (RBER) is obtained by the following equation:

$$\mathrm{RBER} = r_{B,q} \prod_{i=0}^{q-1} P_i\,. \tag{12}$$

Here, $r_{B,q}$ is P_B in the case of a code with rate R_q.

The transfer function *T(D,N)* changes according to the punctured matrices. Further details of the transfer function *T(D,N)* are provided in the Appendix.

Table 1 Number of copies n_i for each pattern under the AWGN channel

i	0	1	2	3	4	$q=5$
Pattern 1, n_i	1	1	1	1	2	4
Pattern 2, n_i	1	2	2	4	4	6
R_i	8/9	4/5	2/3	1/2	1/2	1/2

Table 2 Number of copies n_i for each pattern under the Rayleigh fading channel

i	0	1	2	3	4	$q=5$
Pattern 1, n_i	1	1	1	1	1	3
Pattern 2, n_i	1	3	4	4	5	5
R_i	8/9	4/5	2/3	1/2	1/2	1/2

Table 3 Simulation parameters

Parameter	Detail
Channel model	AWGN
	Rayleigh fading
	IEEE802.15.6 CM3
Modulation	BPSK
FEC	R = 8/9, 4/5, 2/3 and 1/2
	K = 3 convolutional codes
Decoding	Soft decision
	Viterbi decoding
ARQ protocol	Weldon's ARQ
L_{info}	504 bits
Data rate	487 kbps
Roundtrip time	9.84 ms

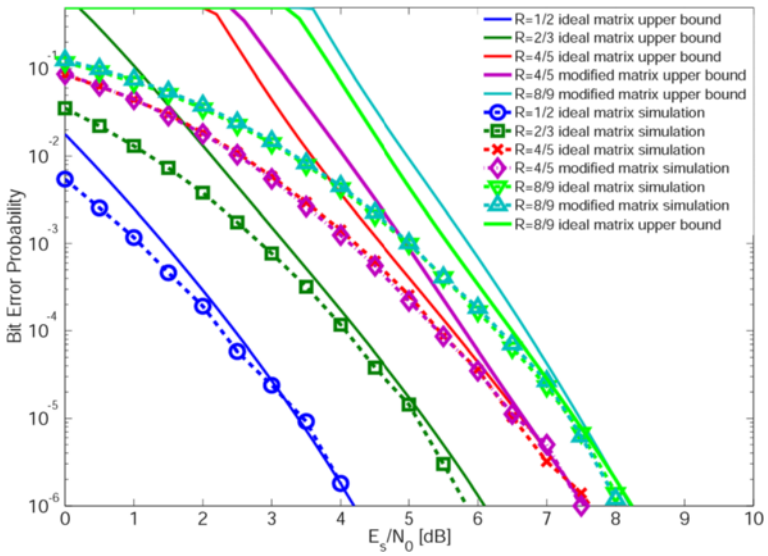

Fig. 6 Bit error probability of punctured convolutional codes under AWGN channel

4 Performance evaluation

4.1 Simulation condition

In this subsection, we evaluate our proposed scheme by theoretical analysis and simulations.

To analyze our proposed scheme, we set two patterns under the AWGN channel and the Rayleigh fading channel, as shown in Tables 1 and 2, respectively. A coding rate of a decomposable code R_i is determined according to the order of Eq. 1. Then, R_i is a coding rate after reconstructing a decomposable code. For the required QoS, the residual BER of pattern 1 is more important than its latency, and the latency of pattern 2 is more important than its residual BER. The number of copies of pattern 1 can achieve the maximum throughput in a high or middle E_s/N_0 area from our theoretical formulae. For pattern 2, the number of copies n_i is large because the latency is allowed; however, the residual BER and throughput performance must be significantly improved. Also, pattern 2 is fixed, as the throughput of pattern 2 is higher than that of the high QoS mode defined in IEEE 802.15.6 (hereinafter called the conventional scheme).

Note that another channel model is assumed to be the Rayleigh fading channel, which is one of the channel models for wearable WBANs [27]. Then, IEEE802.15.6 CM3, which is a typical channel model for wearable WBANs [27], is also assumed in order to evaluate actual performance of our proposed system. This model suffers from strong multipath fading and shadowing. The data rate is referenced from the IEEE802.15.6 standard [17], and the roundtrip time is set based on the data rate and twice the maximum packet length defined in IEEE802.15.6. Simulation parameters are summarized in Table 3.

4.2 Numerical results

Figure 6 shows the bit error probability of the punctured convolutional codes under the AWGN channel. Our proposed punctured convolutional codes with coding rates of 4/5 and 8/9 have a different upper bound than that of the ideal matrix; however, these differences do not significantly influence the performance of our proposed scheme.

Relative to the simulation, the performance of the modified punctured convolutional codes is the same as

Table 4 Optimal number of copies n_i for minimum latency while satisfying PER $\leq 10^{-5}$. Channel model is the AWGN channel

E_s/N_0	n_0	n_1	n_2	n_3
3 dB	1	1	10 $i=q$	–
5 dB	1	7 $i=q$	–	–
6 dB	1	4 $i=q$	–	–
R_i	8/9	4/5	2/3	1/2

Table 5 Optimal number of copies n_i for maximum throughput while satisfying PER $\leq 10^{-5}$. Channel model is the AWGN channel

E_s/N_0	n_0	n_1	n_2	n_3
3 dB	1	1	1	3 $i=q$
5 dB	1	1	2 $i=q$	–
6 dB	1	1	1 $i=q$	–
R_i	8/9	4/5	2/3	1/2

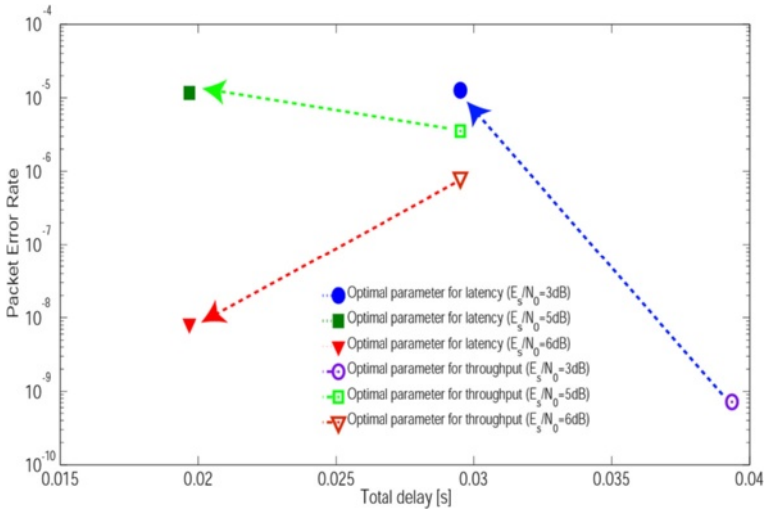

Fig. 7 PER performance with optimal and sub-optimal parameters under AWGN channel. Parameters of Table 4 are optimal

that of the ideal punctured matrices, unlike results of the upper bound. This occurs because the number of trials in the simulation is not large enough. Further, the difference between the error-correcting capacity of the ideal matrix and that of the modified one is very small in the simulation. Hence, the difference does not clearly emerge in the graph without the huge number of trials. The difference between the upper bound and the simulation becomes greater as E_s/N_0 decreases.

Table 4 shows examples of the optimal number of copies n_i for the minimum latency while satisfying PER $\leq 10^{-5}$ by a full search under the AWGN channel. Table 5 shows examples of the optimal number of copies n_i for the maximum throughput while meeting the same condition. Figures 7 and 8 show the theoretical PER and throughput, respectively, according to parameters of Tables 4 and 5. The parameters of Table 4 satisfy the condition that PER $\leq 10^{-5}$ by a smaller delay than Table 5 in Fig. 7, whereas those of Table 5 achieve a larger throughput than that of Table 4 even though a large delay is expected in Fig. 8. In other words, performance with non-optimal parameters in each policy can be considered the same as that of sub-optimal parameters. Then, Figs. 9 and 10 present throughput performances with parameters of Tables 4 and 5 as a function of E_s/N_0. From these figures, we observe that performance changes substantially depending on the parameters. Especially, Fig. 10 shows that each parameter achieves the maximum throughput with the smallest number of retransmissions and n_i copies at each E_s/N_0.

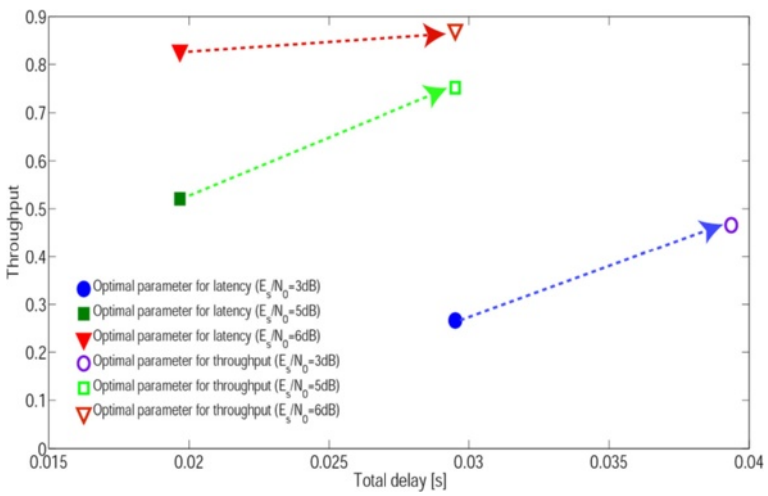

Fig. 8 Throughput performance with optimal and sub-optimal parameters under AWGN channel. Parameters of Table 5 are optimal

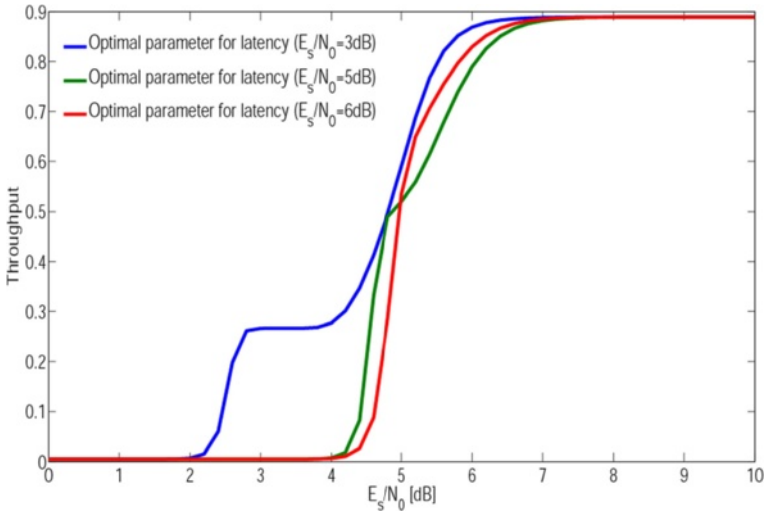

Fig. 9 Throughput performance with parameters of Table 4 under AWGN channel as a function of E_s/N_0

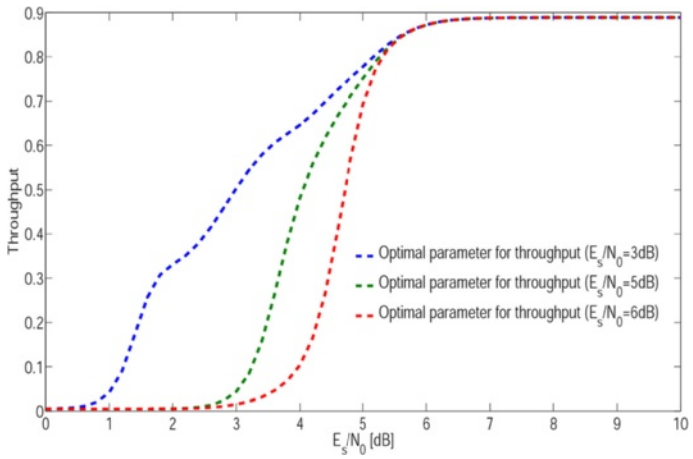

Fig. 10 Throughput performance with parameters of Table 5 under AWGN channel as a function of E_s/N_0

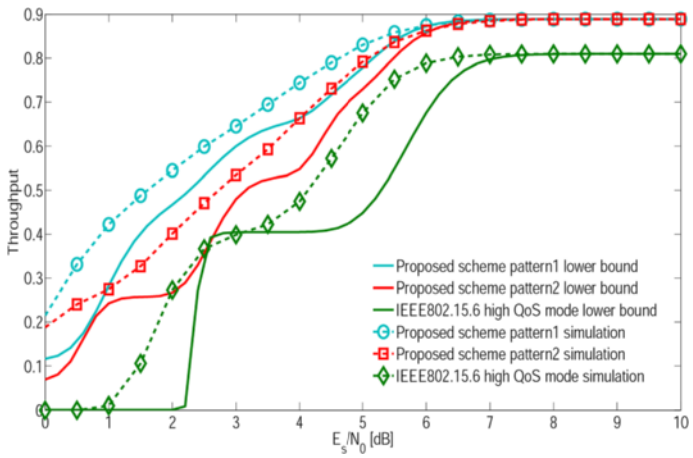

Fig. 11 Throughput performance in the proposed method and the conventional scheme under AWGN channel

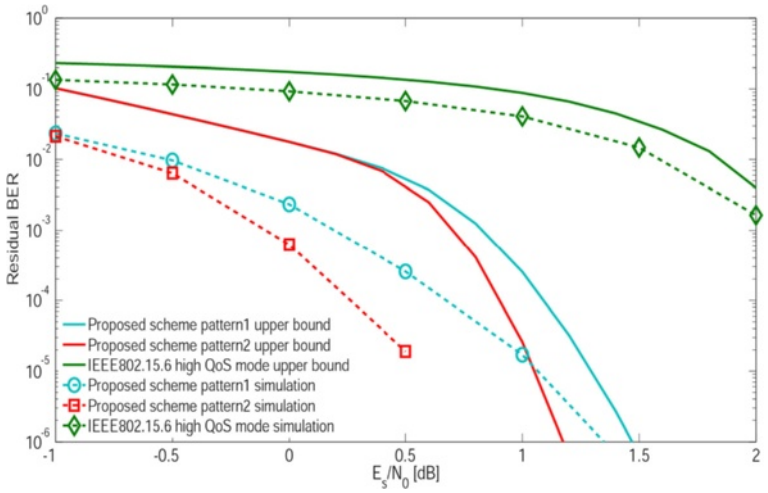

Fig. 12 Residual BER performance in the proposed and the conventional scheme under AWGN channel

Figures 11 and 12 show the throughput and residual BER performance, respectively, for patterns 1 and 2 of our proposed scheme and the conventional scheme under the AWGN channel. Overall, the residual BER performance of our proposed scheme is better than that of the conventional scheme. In the optional pattern, the proposed system obtains over 1.5 dB gain than IEEE802.15.6 system. The throughput of our proposed scheme is also better than that of the conventional scheme. Then, the gain of the proposed scheme is over 1.2 dB gain than that of IEEE802.15.6 scheme in the optional pattern. The throughput and residual BER performances of pattern 1 are opposite to those of pattern 2 because of the parameter settings shown in Table 1. Note that simulation results differ from bounds shown in Fig. 6.

Table 6 shows examples of the optimal number of copies n_i for the minimum latency while satisfying PER $\leq 10^{-5}$ by a full search under the Rayleigh fading channel. And then, Table 7 shows examples of the optimal number of copies n_i for the maximum throughput while meeting the same condition. Figures 13 and 14 express the theoretical PER and throughput, respectively, depending on parameters of Tables 6 and 7. Selected E_s/N_0 is higher than that in the case of the AWGN channel. The reason is that the performance in case of the Rayleigh fading channel is worse than that of the AWGN case. The parameters of Table 6 achieve the condition that PER $\leq 10^{-5}$ by a smaller delay than Table 7 in Fig. 13, whereas those of Table 7 satisfy a larger throughput than Table 6 even though a large delay is needed in Fig. 14. Then, as the case of the AWGN channel, performance with non-optimal parameters in each policy can be regarded as that of sub-optimal parameters. Figures 15 and 16 also present throughput performances with parameters of Tables 6 and 7 as a function of E_s/N_0. From these figures, we can show that performance changes highly according to the parameters like the AWGN case. In particular, Fig. 16 shows that each parameter achieves the maximum throughput with the smallest number of retransmissions and n_i copies at each E_s/N_0.

Figures 17 and 18 present the throughput and residual BER performance, respectively, for patterns 1 and 2 of our proposed scheme and the conventional scheme

Table 6 Optimal number of copies n_i for minimum latency while satisfying PER $\leq 10^{-5}$. Channel model is the Rayleigh fading channel

E_s/N_0	n_0	n_1	n_2	n_3	n_4	n_5
8 dB	1	1	1 $i=q$	3	–	–
11 dB	1	1 $i=q$	4	–	–	–
14 dB	1	7 $i=q$	–	–	–	–
R_i	8/9	4/5	2/3	1/2	1/2	1/2

Table 7 Optimal number of copies n_i for maximum throughput while satisfying PER $\leq 10^{-5}$. Channel model is the Rayleigh fading channel

E_s/N_0	n_0	n_1	n_2	n_3	n_4	n_5
8 dB	1	1	1	1	1	1 $i=q$
11 dB	1	1	1	1	1 $i=q$	–
14 dB	1	1	1	1 $i=q$	–	–
R_i	8/9	4/5	2/3	1/2	1/2	1/2

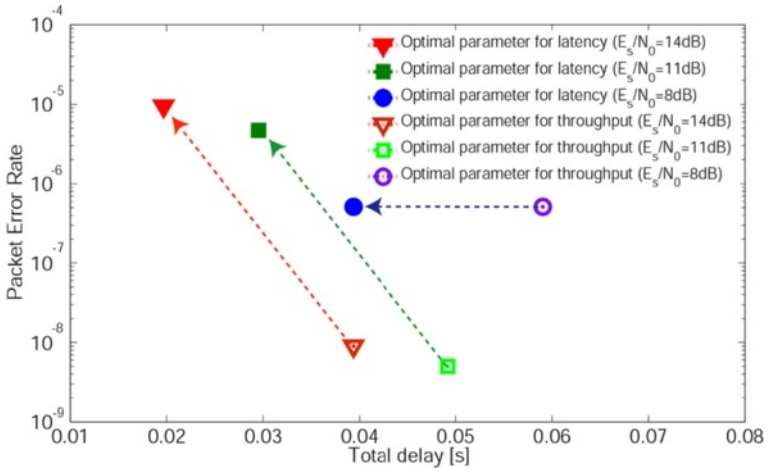

Fig. 13 PER performance with optimal and sub-optimal parameters under the Rayleigh fading channel. Parameters of Table 6 are optimal

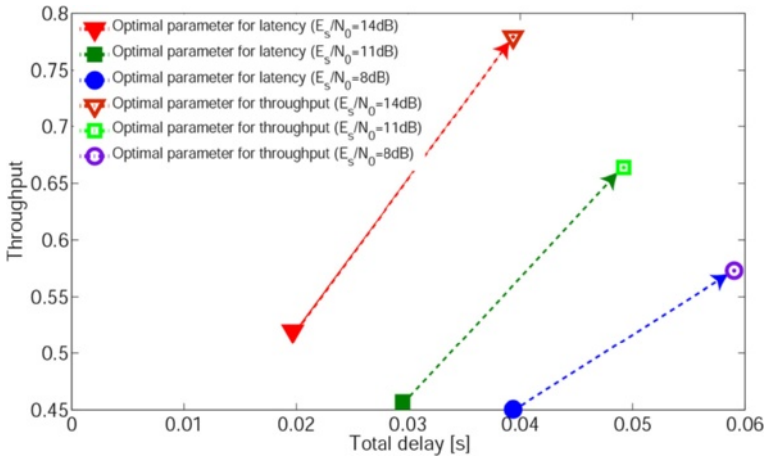

Fig. 14 PER performance with optimal and sub-optimal parameters under the Rayleigh fading channel. Parameters of Table 7 are optimal

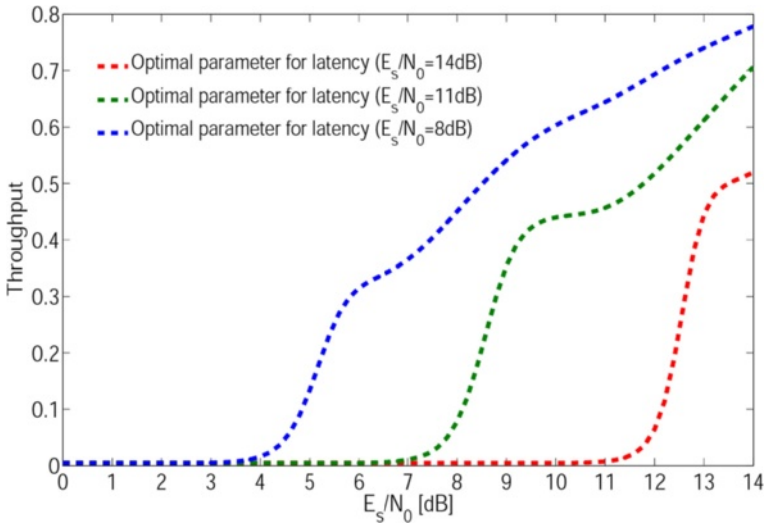

Fig. 15 Throughput performance with parameters of Table 6 under the Rayleigh fading channel as a function of E_s/N_0

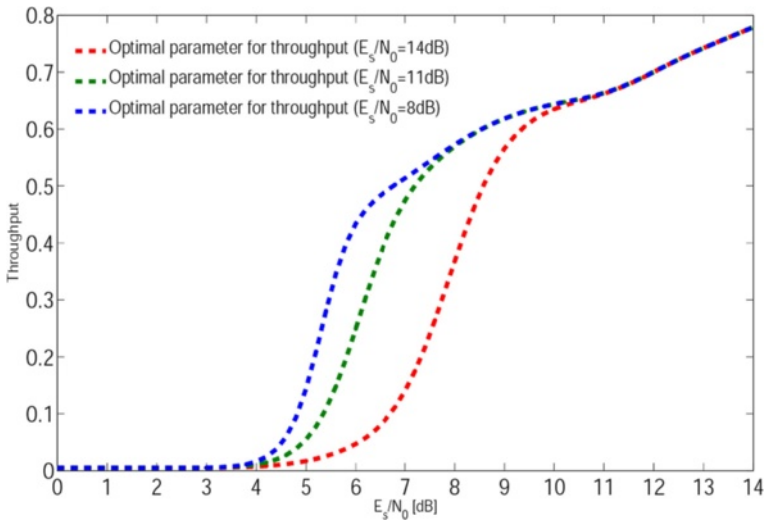

Fig. 16 Throughput performance with parameters of Table 7 under the Rayleigh fading channel as a function of E_s/N_0

under the Rayleigh fading channel. On the whole, our proposed scheme has better residual BER performance than the conventional scheme. In the optional pattern, the proposed system obtains over 4.2 dB gain than the standard system. The throughput of our proposed scheme is also better than that of the conventional scheme. Then, the gain of the proposed scheme is over 4.5 dB gain than that of IEEE802.15.6 in the optional pattern. The throughput and residual BER performances of pattern 1 are also opposite to those of pattern 2 because of the parameter settings shown in Table 2 like the AWGN case. Note that simulation results are different from bounds for the same reason as the case of the AWGN channel.

Figures 19 and 20 show the throughput and residual BER performance, respectively, for two patterns of our proposed scheme and the conventional scheme in the IEEE802.15.6 CM3 channel using simulations as examples of actual performance in a realistic environment. The reason is that it is difficult to theoretically analyze optimal parameters of these schemes in this channel model because the channel model is made by an experiment. Here, parameters are set based on Table 1 as a concrete example. In this channel model, the performance of our proposed scheme is better than that of the conventional scheme. Compared with the AWGN channel and the Rayleigh fading channel, however, the

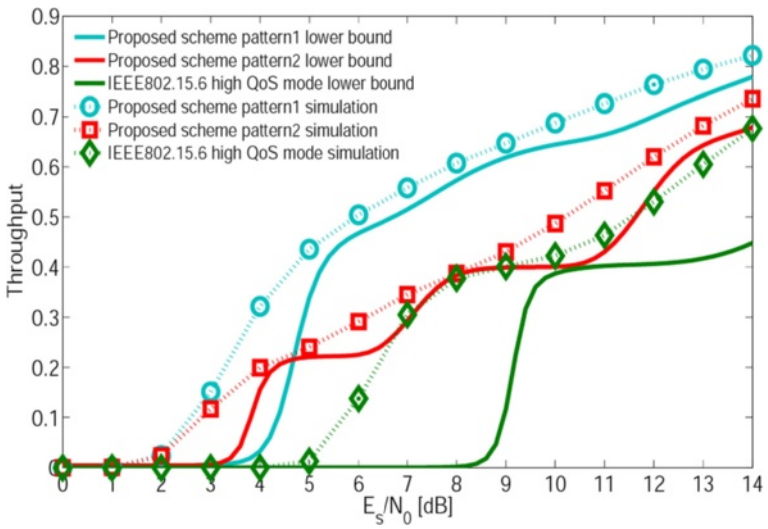

Fig. 17 Throughput performance in the proposed method and the conventional scheme under the Rayleigh fading channel

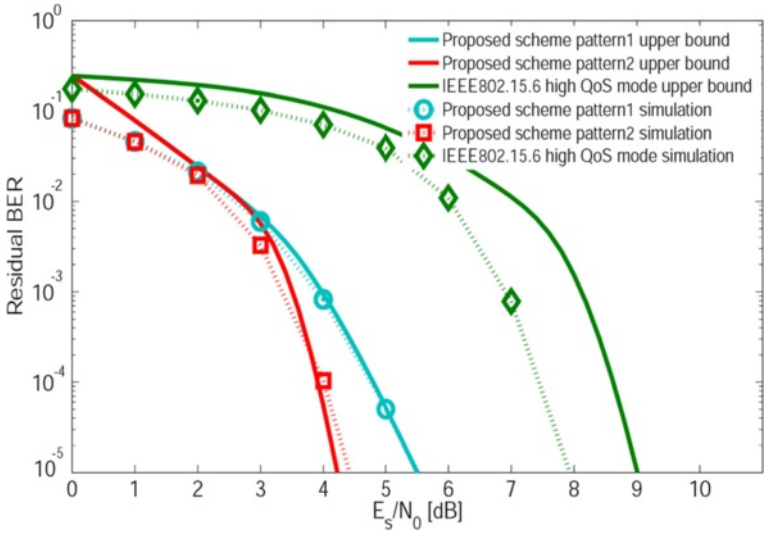

Fig. 18 Residual BER performance in the proposed and the conventional scheme under the Rayleigh fading channel

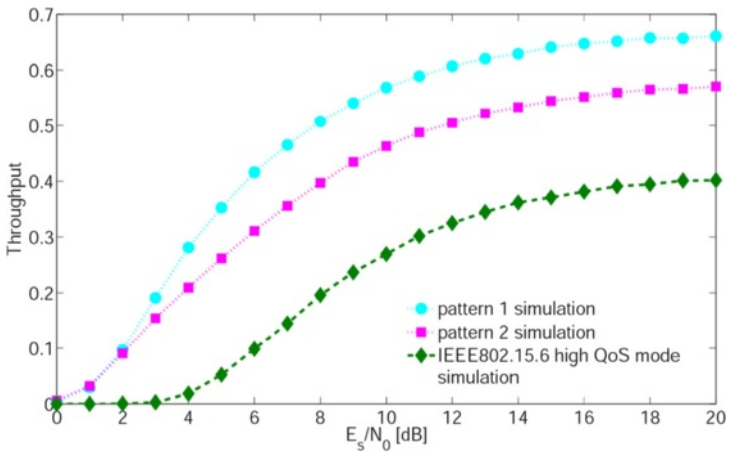

Fig. 19 Throughput performance in proposed and conventional schemes under IEEE802.15.6 CM3

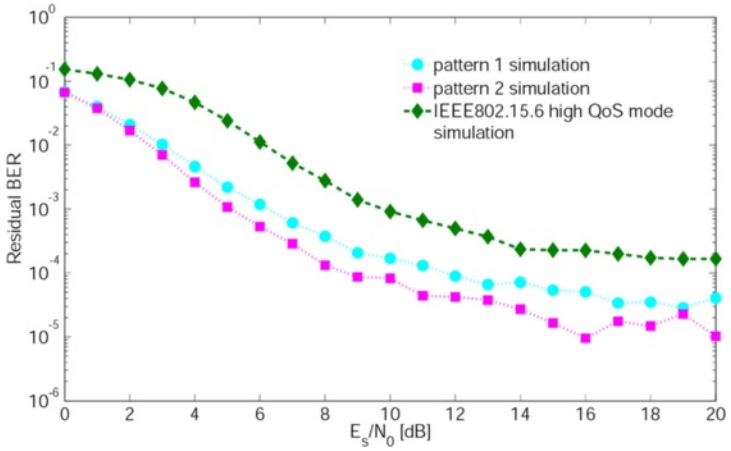

Fig. 20 Residual BER performance in proposed and conventional schemes under IEEE802.15.6 CM3

performance is worse because of the strong multipath fading or shadowing. For this reason, the difference in the performance of our proposed and the conventional schemes is not larger than that of the AWGN channel; however, the tendency of the performance is the same as that of the AWGN channel and the Rayleigh fading channel.

5 Conclusions

In this paper, we presented a theoretical analysis of our proposed scheme to evaluate it under the AWGN channel and the Rayleigh fading channel as an extension of our previous work. We investigated QoS parameters to further optimize our system, showing that our proposed system can achieve optimal performance by arbitrarily selecting parameters of the error-correcting code and Hybrid ARQ. Performance evaluations by theoretical analysis and simulations showed that our proposed scheme has greater flexibility for optimizing QoS parameters according to the required QoS for each input data. Moreover, our evaluations showed that the performance of our proposed scheme is better than that of the conventional scheme.

In the future, we will consider a dynamic channel model and situation such as a multiple WBAN environment that can be theoretically analyzed. Then, optimal parameters for that case should also be investigated.

6 Appendix

6.1 Transfer function

To obtain P_E and P_B, we derive the transfer function $T(D,N)$ from the state diagram using the transfer function technique [24, 25]. Figure 21 shows the state diagram for the punctured convolutional codes.

Here, X_a and X_b express state zero, and the remaining states are arbitrarily labeled X_1, X_2, and X_3. The exponent of N indicates the number of information bits set to "1" that causes the transition to occur, and the exponent of D indicates the Hamming weight on the transition. From Fig. 21, the matrix equation is given as follows:

$$\begin{bmatrix} X_1 \\ X_2 \\ X_3 \end{bmatrix} = \begin{bmatrix} g_{11} & g_{12} & g_{13} \\ g_{21} & g_{22} & g_{23} \\ g_{31} & g_{32} & g_{33} \end{bmatrix} \begin{bmatrix} X_1 \\ X_2 \\ X_3 \end{bmatrix} + \begin{bmatrix} (N^3+N^2+N)D^2+N^2D^4 \\ (N^2+N)D+N^3D^3+N^2D^5 \\ N^2D+(N^4+2N^3)D^3 \end{bmatrix} X_a \tag{13}$$

$$\begin{cases} g_{11} = N^3+N^2D^2+(N^2+N)D^4 \\ g_{12} = (N^3+2N^2)D^2+ND^4 \\ g_{13} = (N^3+2N^2)D^2+ND^4 \\ g_{21} = N^3D+(2N^2+N)D^3 \\ g_{22} = N^2D+(N^3+N^2+N)D^3 \\ g_{23} = N^2D+(N^3+N^2+N)D^3 \\ g_{31} = N^7D+N^3D^3+N^2D^5 \\ g_{32} = N^3D+(N^4+N^3+N^2)D^3 \\ g_{33} = N^3D+(N^4+N^3+N)D^3 \end{cases} \tag{14}$$

$$\boldsymbol{X} = \boldsymbol{A}\boldsymbol{X} + \boldsymbol{F}X_a \tag{15}$$

$$X_b = \begin{bmatrix} (N^2+N+1)D^2+ND^4 \\ (2N^2+1)D^2+N^2D^4 \\ (2N^2+1)D^2+N^2D^4 \end{bmatrix}^T \begin{bmatrix} X_1 \\ X_2 \\ X_3 \end{bmatrix} + \{N^2D^2+(N^2+N)D^4\}X_a \tag{16}$$

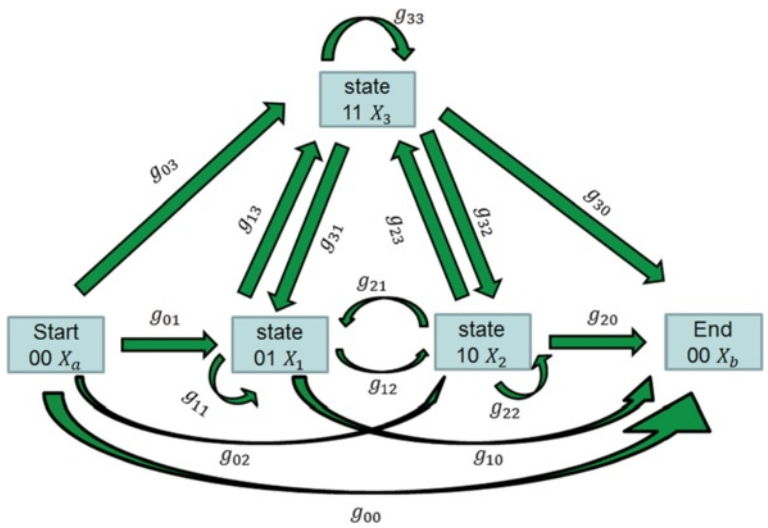

Fig. 21 State diagram of punctured convolutional codes

$$X_b = \boldsymbol{G}\boldsymbol{X} + hX_a. \tag{17}$$

As above, the transfer function is given as follows:

$$\begin{aligned} T(D,N) = \frac{X_a}{X_b} &= \boldsymbol{G}[\boldsymbol{I}-\boldsymbol{A}]^{-1}\boldsymbol{F} + h \\ &= h + \boldsymbol{G}\boldsymbol{F} + \boldsymbol{G}\boldsymbol{A}\boldsymbol{F} + \boldsymbol{G}\boldsymbol{A}^2\boldsymbol{F} + \boldsymbol{G}\boldsymbol{A}^3\boldsymbol{F} + \dots . \end{aligned} \tag{18}$$

Thus, coefficient c_d is given as follows:

$$\begin{aligned} \frac{dT(D,N)}{dN}\Big|_{N=1} &= \sum_{d=d_{free}}^{\infty} c_d D^d \\ &= D^2 + 21D^3 + 1872D^4 + 9127D^5 \\ &\quad + 40922D^6 + 206380D^7 + 871148D^8 \\ &\quad + 3372445D^9 + 12553649D^{10} \\ &\quad + 43727850D^{11} + \dots . \end{aligned} \tag{19}$$

For coding rate 8/9, we obtain its transfer function using the same procedure:

$$\begin{cases} h = g_{00} \\ \boldsymbol{G} = [\,g_{01} \quad g_{02} \quad g_{03}\,] \\ \boldsymbol{F} = \begin{bmatrix} g_{10} \\ g_{20} \\ g_{30} \end{bmatrix} \\ \boldsymbol{A} = \begin{bmatrix} g_{11} & g_{12} & g_{13} \\ g_{21} & g_{22} & g_{23} \\ g_{31} & g_{32} & g_{33} \end{bmatrix} \end{cases} \tag{20}$$

$$\begin{cases} g_{00}=N^4D^9+(N^5+N^4+4N^3+N^2)D^7 \\ \quad +(N^6+2N^5+N^4+3N^3+2N^2)D^6 \\ \quad +(N^5+6N^4+4N^3+3N^2)D^5+(2N^5+6N^4+3N^3+3N^2)D^4 \\ \quad +(3N^3+2N^2+N)D^3+(2N^3+N^2+N)D^2 \\ g_{01}=N^3D^8+(2N^5+5N^4+2N^3)D^7+(4N^4+2N^3)D^6 \\ \quad +(2N^6+5N^5+3N^4+4N^3+N^2)D^5 \\ \quad +(N^7+3N^6+5N^5+N^4+3N^3+N^2)D^4 \\ \quad +(N^5+3N^4)D^3+(N^6+2N^5+3N^4)D^2 \\ g_{02}=(N^5+2N^4+N^3)D^8+(N^4+N^3)D^7+(N^6+3N^5+4N^4+2N^3)D^6 \\ \quad +(N^7+3N^6+4N^5+4N^4+3N^3)D^5+(N^6+4N^5+4N^4+3N^3+N^2)D^4 \\ \quad +(N^6+3N^5+2N^4+2N^3+N^2)D^3+N^4D^2+N^4D \\ g_{03}=(N^6+N^5)D^8+(2N^5+2N^4)D^7+(2N^7+5N^6+6N^5+3N^4)D^6 \\ \quad +(N^8+2N^7+2N^6+2N^5+2N^4)D^5+(2N^6+3N^5+3N^4+N^3)D^4 \\ \quad +(2N^7+5N^6+3N^5+2N^4+N^3)D^3+N^5D^2+N^5D \end{cases} \tag{21}$$

$$\begin{cases} g_{10}=N^5D^8+(3N^4+4N^3+2N^2)D^7+(3N^4+2N^3+2N^2)D^6 \\ \quad +(N^5+N^4+6N^3+5N^2+2N)D^5+(N^6+N^5+N^4+5N^3+4N^2+3N)D^4 \\ \quad +(N^5+4N^4+N^3+N^2)D^3+(2N^5+3N^4+N^3+N^2)D^2+N^3D \\ g_{11}=N^4D^9+(N^5+N^4+4N^3+N^2)D^7+(N^6+N^5+N^4+4N^3+2N^2)D^6 \\ \quad +(3N^5+8N^4+3N^3+N^2)D^5+(2N^5+7N^4+3N^3+N^2)D^4 \\ \quad +(2N^6+4N^5+2N^4+N^3)D^3+(N^7+2N^6+4N^5)D^2+N^6 \\ g_{12}=(N^4+N^3)D^8+(N^6+N^5+N^4+N^3)D^7+(3N^5+6N^4+5N^3+2N^2)D^6 \\ \quad +(2N^5+3N^4+3N^3+2N^2)D^5+(N^6+3N^5+4N^4+2N^3)D^4 \\ \quad +(N^7+2N^6+3N^5+4N^4+3N^3+N^2)D^3+(N^6+2N^5+N^4)D^2+(N^6+N^5)D \\ g_{13}=(N^6+2N^5+N^4)D^8+(N^7+N^4)D^7+(2N^6+4N^5+3N^4+N^3)D^6 \\ \quad +(3N^6+5N^5+5N^4+3N^3)D^5+(2N^7+4N^6+5N^5+4N^4+N^3)D^4 \\ \quad +(N^8+N^7+2N^6+3N^5+N^4)D^3+(N^6+N^5)D^2+(2N^7+2N^6)D \end{cases} \tag{22}$$

$$\begin{cases} g_{20}=(N^5+2N^4+2N^3+N^2)D^7+(N^6+N^5+N^4+2N^3+N^2)D^6 \\ \quad +(N^5+5N^4+7N^3+5N^2+2N)D^5+(3N^5+5N^4+5N^3+5N^2+2N)D^4 \\ \quad +(N^4+3N^3+2N^2)D^3+(N^4+N^3+N^2+N)D^2 \\ g_{21}=(N^5+2N^4+2N^3+N^2)D^7+(2N^4+3N^3+N^2)D^6 \\ \quad +(2N^6+5N^5+7N^4+5N^3+N^2)D^5+(N^7+2N^6+4N^5+5N^4+4N^3+2N^2)D^4 \\ \quad +(2N^5+3N^4+N^3)D^3+(2N^6+3N^5+N^4)D^2 \\ g_{22}=N^4D^8+N^3D^7+(N^6+4N^5+3N^4+5N^3+2N^2)D^6 \\ \quad +(N^7+2N^6+3N^5+6N^4+2N^3+N^2)D^5+(N^6+3N^5+8N^4+3N^3)D^4 \\ \quad +(2N^6+4N^5+N^4+4N^3+2N^2)D^3+N^5D^2+N^4D \\ g_{23}=N^4D^8+N^5D^7+(2N^7+5N^6+6N^5+N^4+N^3)D^6 \\ \quad +(N^8+N^7+2N^6+3N^5+6N^4+2N^3)D^5+(3N^6+5N^5+6N^4+N^3)D^4 \\ \quad +(3N^7+4N^6+4N^5+N^4+N^3)D^3+N^5D^2+N^6D \end{cases} \tag{23}$$

$$\begin{cases} g_{30}=(N^5+2N^4+2N^3+N^2)D^7+(N^6+N^5+N^4+2N^3+N^2)D^6 \\ \quad +(N^5+5N^4+7N^3+5N^2+2N)D^5+(3N^5+5N^4+5N^3+5N^2+2N)D^4 \\ \quad +(N^4+3N^3+2N^2)D^3+(N^4+N^3+N^2+N)D^2 \\ g_{31}=(N^5+2N^4+2N^3+N^2)D^7+(2N^4+3N^3+N^2)D^6 \\ \quad +(2N^6+5N^5+7N^4+5N^3+N^2)D^5+(N^7+2N^6+4N^5+5N^4+4N^3+2N^2)D^4 \\ \quad +(2N^5+3N^4+N^3)D^3+(2N^6+3N^5+N^4)D^2 \\ g_{32}=N^4D^8+N^3D^7+(N^6+4N^5+3N^4+5N^3+2N^2)D^6 \\ \quad +(N^7+2N^6+3N^5+6N^4+2N^3+N^2)D^5+(N^6+3N^5+8N^4+3N^3)D^4 \\ \quad +(2N^6+4N^5+N^4+4N^3+2N^2)D^3+N^5D^2+N^4D \\ g_{33}=N^4D^8+N^5D^7+(2N^7+5N^6+6N^5+N^4+N^3)D^6 \\ \quad +(N^8+N^7+2N^6+3N^5+6N^4+2N^3)D^5+(3N^6+5N^5+6N^4+N^3)D^4 \\ \quad +(3N^7+4N^6+4N^5+N^4+N^3)D^3+N^5D^2+N^6D \end{cases} \tag{24}$$

From the matrices, c_d is given in the same way as follows:

$$\begin{aligned} \frac{dT(D,N)}{dN}\Big|_{N=1} &= \sum_{d=d_{free}}^{\infty} c_d D^d \\ &= 9D^2 + 1780D^3 + 17036D^4 \\ &\quad + 164093D^5 + 1463387D^6 \\ &\quad + 11239801D^7 + 80280102D^8 \\ &\quad + 535025955D^9 + 3323529844D^{10} \\ &\quad + 19393645707D^{11} + \dots . \end{aligned} \tag{25}$$

For coding rates 1/2 and 2/3, we use the transfer functions in reference [25] because their coefficients are the same in the case of ideal punctured matrices. Here, $R = 1/2$ is enumerated as follows:

$$\begin{aligned} \frac{dT(D,N)}{dN}\Big|_{N=1} &= \sum_{d=d_{free}}^{\infty} c_d D^d \\ &= \sum_{d=d_{free}}^{\infty} \left(d - d_{free} + 1\right) 2^{d-d_{free}} D^d. \end{aligned} \tag{26}$$

And, $R = 2/3$ is represented as follows:

$$\begin{aligned} \frac{dT(D,N)}{dN}\Big|_{N=1} &= \sum_{d=d_{free}}^{\infty} c_d D^d \\ &= D^3 + 10D^4 + 54D^5 + 226D^6 \\ &\quad + 856D^7 + 3072D^8 + 10647D^9 \\ &\quad + 35998D^{10} + 119478D^{11} + \dots . \end{aligned} \tag{27}$$

Competing interests
The authors declare that they have no competing interests.

Acknowledgements
The first author would like to thank members of Kohno laboratory, Yokohama National University, Japan for their great inspiration and kindness.

Author details
[1]Graduate School of Engineering, Yokohama National University, 79-5 Tokiwadai, Hodogaya-Ku, 240-8501 Yokohama, Japan. [2]Graduate School of Information Sciences, Hiroshima City University, 3-4-1, Ozuka-Higashi, Asa-Minami-Ku, 731-3194 Hiroshima, Japan.

Received: 6 September 2015 Accepted: 18 February 2016

References

1. M Chen, S Gonzalez, A Vasilakos, H Cao, VCM Leung, Body area networks: a survey. Mobile Networks and Applications, Springer **16**(2), 171–193 (2010)
2. G Acampora, DJ Cook, P Rashidi, AV Vasilakos, A survey on ambient intelligence in healthcare. Proc. IEEE **101**(12), 2470–2494 (2013)
3. T Hayajneh, G Almashaqbeh, S Ullah, AV Vasilakos, A survey of wireless technologies coexistence in WBAN: analysis and open research issues. Wireless Networks, Springer **20**(8), 2165–2199 (2014)
4. G Fortino, GD Fatta, M Pathan, AV Vasilakos, Cloud-assisted body area networks: state-of-the-art and future challenges. Wireless Networks, Springer **20**(7), 1925–1938 (2014)
5. J Zhou, Z Cao, X Dong, X Lin, AV Vasilakos, Securing m-healthcare social networks: challenges, countermeasures and future directions. Wireless Communications, IEEE **20**(4), 12–21 (2013)
6. J Zhou, Z Cao, X Dong, N Xiong, AV Vasilakos, 4S: a secure and privacy-preserving key management scheme for cloud-assisted wireless body area network in m-healthcare social networks. Information Sciences, Elsevier **314**(2015), 255–276 (2014)
7. D He, C Chen, S Chan, J Bu, AV Vasilakos, ReTrust: attack-resistant and lightweight trust management for medical sensor networks. Transactions on Information Technology in Biomedicine, IEEE **16**(4), 623–632 (2012)
8. Z Zhang, H Wang, AV Vasilakos, H Fang, ECG-cryptography and authentication in body area networks. Transactions on Information Technology in Biomedicine, IEEE **16**(6), 1070–1078 (2012)
9. D Lin, F Labeau, AV Vasilakos, QoE-based optimal resource allocation in wireless healthcare networks: opportunities and challenges. Wireless Networks, Springer **21**(8), 2483–2500 (2015)
10. H Cao, V Leung, C Chow, H Chan, Enabling technologies for wireless body area networks: a survey and outlook. IEEE Comm. Mag. **47**(12), 84–93 (2009)
11. H Viswanathan, B Chen, D Pompili, Research challenges in computation, communication, and context awareness for ubiquitous healthcare. IEEE Comm. Mag. **50**(5), 92–99 (2012)
12. C Bachmann, M Ashouei, V Pop, M Vidojkovic, HD Groot, B Gyselinckx, Low-power wireless sensor nodes for ubiquitous long-term biomedical signal monitoring. IEEE Comm. Mag. **50**(1), 20–27 (2012)
13. JMLP Caldeira, JJPC Rodrigues, P Lorenz, Toward ubiquitous mobility solutions for body sensor networks on healthcare. IEEE Comm. Mag. **50**(5), 108–115 (2012)
14. A Boulis, D Smith, D Miniutti, L Libman, Y Tselishchev, Challenges in body area networks for healthcare: the MAC. IEEE Comm. Mag. **50**(5), 100–106 (2012)
15. A Wong, M Dawkins, G Devita, N Kasparidis, A Katsiamis, O King, F Lauria, J Schiff, A Burdett, *A 1V 5mA Multimode IEEE 802.15.6/Bluetooth Low-Energy WBAN Transceiver for Biotelemetry Applications. Proceedings of Solid-State Circuits Conference Digest of Technical Papers (ISSCC), 2012 IEEE International*, 2012, pp. 300–302
16. T Suzuki, H Tanaka, S Minami, H Yamada, T Miyata, *Wearable wireless vital Monitoring Technology for Smart Health Care. Proceedings of 7th International Symposium on Medical Information and Communication Technology (ISMICT): March 2013; Tokyo, Japan*, 2013
20. IEEE Standard for Information technology - Telecommunications and information exchange between systems - Local and metropolitan area networks- Specific requirements: Part 15.6: Wireless Medium Access Control (MAC) and Physical Layer (PHY) Specifications for Wireless Personal Area Networks (WPANs) used in or 12 around a body. IEEE (2011)
18. IEEE Standard for Local and metropolitan area networks Part 15.4: Low-Rate Wireless Personal Area Networks (LR-WPANs), Amendment: Alternative Physical Layer Extension to support Medical Body Area Networks (MBANS) services operating in the 2360–2400 MHz band. IEEE (2013)
20. ETSI TC Smart BAN: SmartBAN System Description. TR DTS/SmartBAN-008 V0.1.0 (2014)
20. K Takabayashi, H Tanaka, C Sugimoto, R Kohno, *An Error Control Scheme with Weldon's ARQ Considering Various QoS in Medical and Non-medical Uses for Wireless BANs. Proceedings of 7th International Symposium on Medical Information and Communication Technology (ISMICT): March 2013; Tokyo, Japan*, 2013
21. K Takabayashi, H Tanaka, C Sugimoto, R Kohno, *Multiplexing and Error Control Scheme with Modified Hybrid ARQ for Body Area Network employing IEEE 802.15.6 in UWB-PHY. Proceedings of 8th International Conference on Body Area Networks (BodyNets 2013): September 2013; Boston, Massachusetts, United States*, 2013
22. K Takabayashi, H Tanaka, C Sugimoto, R Kohno, *Multiplexing and Error Control Scheme for Body Area Network employing IEEE 802.15.6. Transactions on Communications, IEICE E97-B(03)*, 2014, pp. 564–570
25. E Weldon Jr, An improved selective-repeat ARQ strategy. IEEE Trans. Comm. **30**(3), 480–486 (1982)
24. AJ Viterbi, Convolutional codes and their performance in communication systems. Transactions on Communication Technology, IEEE **19**(5), 751–772 (1971)
25. D Haccoun, G Begin, High-rate punctured convolutional codes for viterbi and sequential decoding. IEEE Trans. Comm. **37**(11), 1113–1125 (1989)
26. P Franger, P Orten, T Ottosson, Convolutional codes with optimum distance spectrum. IEEE Commun. Lett. **3**(11), 317–319 (1999)
27. KY Yazdandoost, K Sayrafian-Pour, *Channel Model for Body Area Network (BAN). IEEE P802.15 Working Group for Wireless Per-sonal Area Networks(WPANs), IEEE P802.15-08-0780-10-0006*, 2009